Wind observations with Doppler weather radar

Iwan Holleman
Royal Netherlands Meteorological Institute (KNMI),
PO Box 201, NL-3730AE De Bilt, Netherlands,
Email: holleman@knmi.nl

I. Introduction

Weather radars are commonly employed for detection and ranging of precipitation, but radars with Doppler capability can also provide detailed information on the wind associated with (severe) weather phenomena. The Royal Netherlands Meteorological Institute (KNMI) operates two identical C-band (5.6 GHz) Doppler weather radars. One radar is located in De Bilt and the other one is located in Den Helder. Two distinctly different pulse repetition frequencies are used to extend the unambiguous velocity interval of the Doppler radars from 13 to 40 m/s (Holleman 2003). In this paper, the retrieval and quality of weather radar wind profiles are discussed. In addition the extraction of temperature advection from these profiles is presented. Finally the detection of severe weather phenomena and monitoring of bird migration for aviation are highlighted.

II. Retrieval of radar wind profiles

A Doppler weather radar measures the scattering from atmospheric targets, like rain, snow, dust, and insects. The radar provides the mean radial velocity as a function of range, azimuth, and elevation. Assuming a uniform wind field (u_0,v_0,w_0) and a constant fall velocity, the radial velocity V_r can be modelled as a function of the azimuth ϕ and the elevation θ:

$$V_r(\phi,\theta) = u_0 \cos\theta \sin\phi + v_0 \cos\theta \cos\phi + w_0' \sin\theta \qquad (1)$$

where w_0' is the sum of the vertical wind speed and the terminal fall velocity of the hydrometeors. When Doppler data are displayed at constant range and elevation, the radial velocity as a function of azimuth will resemble a sine (see Figure 1). The wind speed and direction can be determined from the amplitude and the phase of the sine, respectively. This well-known technique is called Velocity Azimuth Display (VAD) and was introduced by Browning and Wexler in 1968.

Instead of processing multiple VADs and averaging the results, one can also process all available radial velocity data within a certain height layer at once. The parameters of the wind field can then be extracted using a multi-dimensional and multi-parameter linear fit. This so-called Volume Velocity Processing technique (VVP) has been introduced by Waldteufel and Corbin in 1979. At KNMI the VVP technique is used for the operational production of weather radar wind profiles with a 200 m height resolution (Holleman 2005).

Figure 1 shows two examples of VAD data from the operational weather radar in De Bilt. The huge difference

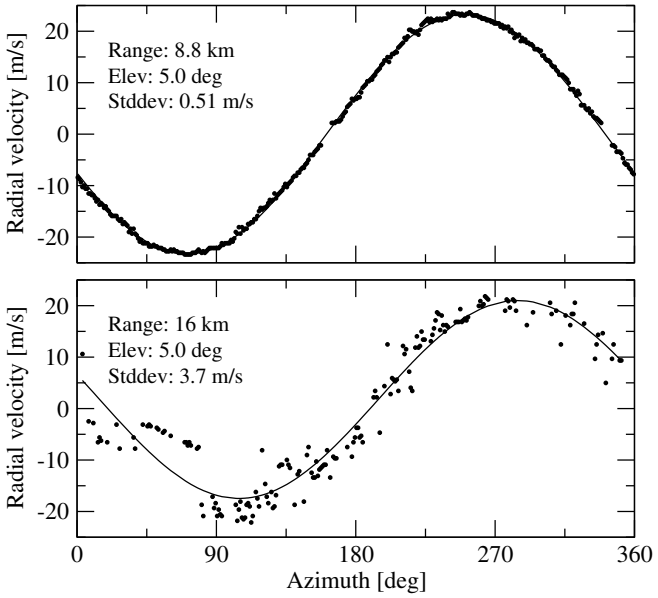

Fig. 1. Two examples of Velocity Azimuth Display (VAD) data from the operational weather radar in De Bilt are shown. The upper frame displays a VAD during the passage of a cold front (1409 UTC on 8 March 2003) and the lower frame during intense bird migration (0009 UTC on 7 March 2003).

in scatter of the observed radial velocity data around the modelled radial velocities is evident (the origin is discussed below). The amount of scatter can be quantified using the standard deviation of the radial velocity (σ_r):

$$\sigma_r^2 = \frac{1}{N-3} \sum_{i=1}^{N} [V_{r,i} - V_r(\phi_i,\theta_i)]^2 \qquad (2)$$

where $V_{r,i}$ are the observed radial velocities and N is the number of data points. Quality control on the wind data is performed by rejecting all vectors with a σ_r above 2.0 m/s.

III. Verification of radar wind profiles

An intercomparison of different implementations of the VAD and VVP wind profile retrieval methods using radiosonde profiles as a reference revealed that the VVP method performs slightly better than the VAD method (Holleman 2005). Furthermore it was found that the simplest implementation of the VVP retrieval method, i.e., using the uniform wind field, provides the best horizontal wind data.

Figure 2 shows the statistics of the VVP (upper frames) and radiosonde (lower frames) wind profile observations against

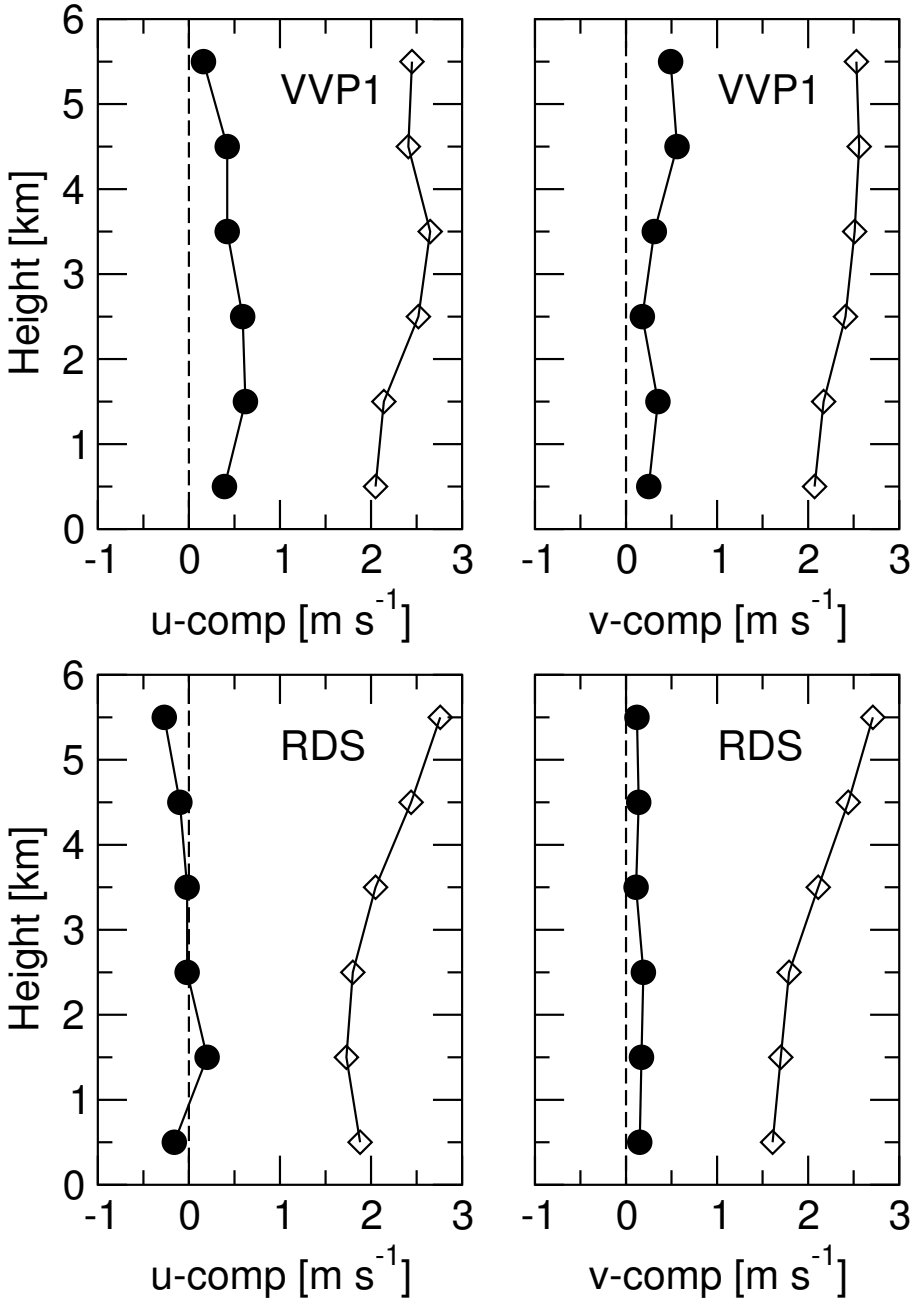

Fig. 2. Profiles of the bias (●) and standard deviation (◇) of the Cartesian u- and v-components from the verification of the radar (upper) and radiosonde (lower) wind data against the HIRLAM NWP model.

the HIRLAM NWP background. The bias and standard deviation of the Cartesian u- and v-components of the wind vectors are calculated for a 9 months verification period. In this comparison the radiosonde has a clear advantage over weather radar because the radiosonde profiles are assimilated by the HIRLAM model. For the radar wind data, a small positive bias for both Cartesian components is seen.

Quality differences between the weather radar (VVP) and radiosonde observations can be assessed by investigating the standard deviation of the observations against the HIRLAM background. The standard deviation of the radiosonde wind vector components is between 1.5 and 2.0 m/s at ground level and gradually increases to almost 3.0 m/s aloft. This increase is probably due to the increase of the wind speeds with height and to horizontal drifting of the radiosonde. The standard deviation of the VVP wind vector components against the HIRLAM background is around 2.0 m/s at ground level and only 2.5 m/s aloft. Figure 2 shows that observation minus background statistics of the weather radar wind profiles are at least as good as those of the radiosonde profiles. This result clearly demonstrates the high quality of the weather radar wind profiles.

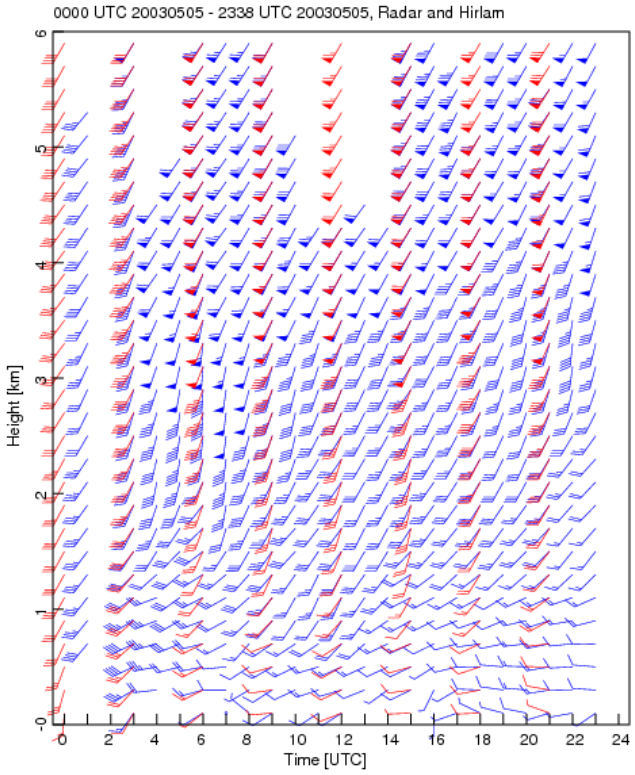

Fig. 3. A time-height plot with the weather radar wind profiles (blue barbs) for 5 May 2003. The wind profiles from the HIRLAM NWP model are overlaid in red. Wind speed and direction are indicated by wind vanes. Each full barb represents a wind speed of 5 m/s and each triangle a wind speed of 25 m/s.

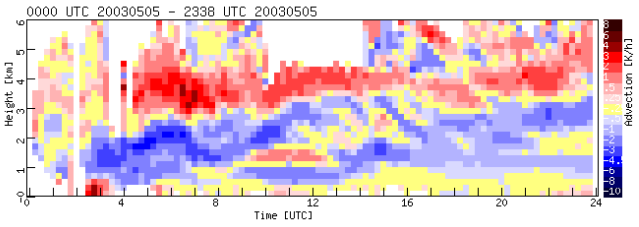

Fig. 4. Time-height plot of temperature advection calculated from radar wind profile data of 5 May 2003 (see Figure 3). Red indicates advection of warm air and blue of cold air.

IV. Temperature Advection from Thermal Wind

Figure 3 shows a time-height plot of the weather radar and HIRLAM wind profiles during the passage of a cold front. Evidently the agreement between the radar and model wind vectors is good, but the update frequency and availability differ. The vertical shear in the wind profiles can be highlighted by deducing the temperature advection using the thermal wind. The thermal wind (u_T,v_T), which is basically the vertical shear of the (geostrophic) wind, is given by:

$$v_T = -\frac{R}{f}\ln(p_2/p_1)\left(\frac{\partial T}{\partial x}\right)_p \tag{3}$$

where R and f are the ideal gas constant and the Coriolis parameter, p_1 and p_2 are the air pressures at the bottom and top of the height layer. A similar equation is valid for u_T. Assuming hydrostatic balance one can calculate the temperature gradients from the vertical wind shear:

$$\frac{\partial T}{\partial x} = +\frac{f}{g}\left(\frac{v_2 - v_1}{z_2 - z_1}\right)T(\bar{z}) \tag{4}$$

$$\frac{\partial T}{\partial y} = -\frac{f}{g}\left(\frac{u_2 - u_1}{z_2 - z_1}\right)T(\bar{z}) \tag{5}$$

Where g is the gravitational constant, $\bar{z}$ the mean height of the layer $(z_1 + z_2)/2$ and the temperature $T(z)$ is approximated by the International Standard Atmosphere (ISA). Thus the temperature advection is obtained from:

$$\frac{\partial T}{\partial t} = -\left(u\frac{\partial T}{\partial x} + v\frac{\partial T}{\partial y}\right) \tag{6}$$

The temperature advection has been calculated from the wind profiles in Figure 3 and the result is shown in Figure 4. Cold air advection (blue) is seen below 3 km and warm air advection (red) is found above. This can be explained by the cold front arching backward. Because the front is moving slowly, the cold advection does not penetrate heights above 3 km, something that would normally occur if the front was moving faster (Jonker 2003).

The temperature advection is retrieved using the geostrophic approximation which is questionable for mesoscale phenomena. Nevertheless, displaying the temperature advection emphasizes the rotation and vertical shear in the wind field, which would probably stay unnoticed otherwise.

V. Mesocyclones Detected with Horizontal Wind Shear

Mesoscale severe weather phenomena like gust fronts, microbursts, and mesocylcones, are usually associated with small-scale deviations in the local wind field. These small-scale deviations can be accentuated by calculation of the horizontal shear (HZS). The horizontal shear is a combination of the so-called radial shear (RS) and the azimuthal shear (AS). The radial shear is calculated by differencing the observed Doppler velocities at different ranges from the radar while the azimuth shear is calculated from different azimuths (Holleman et al. 2005). The horizontal shear is then calculated from:

$$\mathrm{HZS} = \sqrt{\mathrm{RS}^2 + \mathrm{AS}^2} \tag{7}$$

Values above 8 m s^{-1} km^{-1} indicate severe and/or dangerous shear zones.

On 23 August 2004 a cold front passed over the Netherlands from southwest to northeast and around 15 UTC a supercell thunderstorm developed on this front. Around 16 UTC the supercell produced a tornado near Muiden. Figure 5 shows the damage inflicted on an old barn in Muiden. The supercell

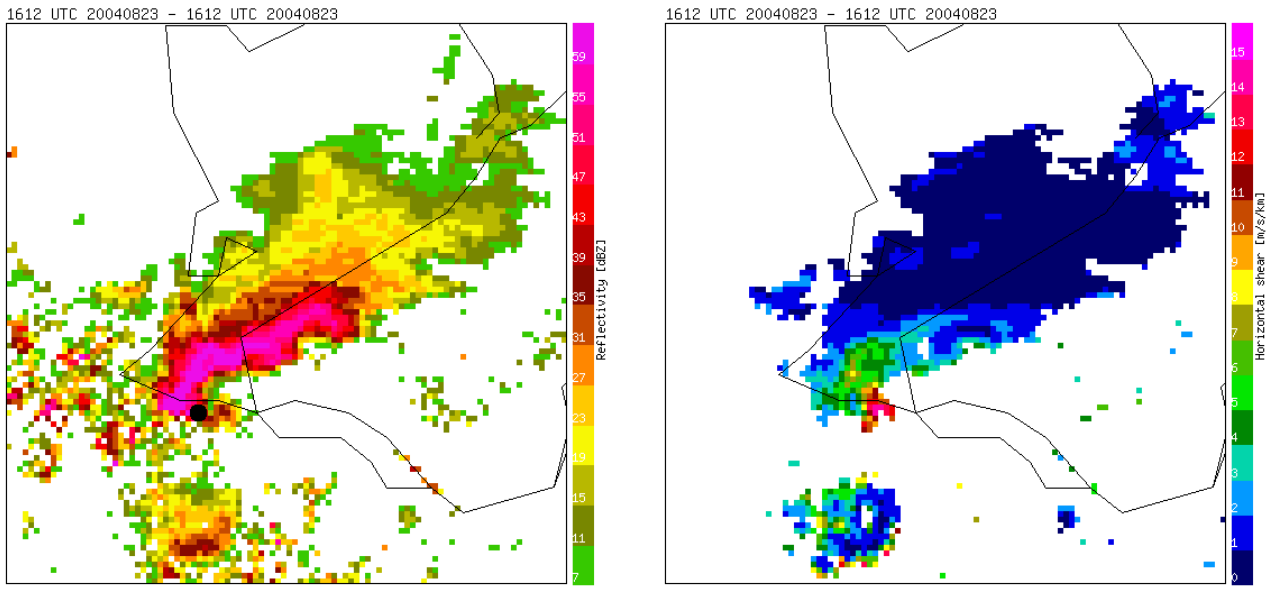

Fig. 6. Part (a) shows a high-resolution (0.5 km) reflectivity product recorded by the Doppler radar in De Bilt at 0.3 deg elevation and zoomed around the supercell (1612 UTC on 23 August 2004) over Muiden (marked by black dot, west of Amsterdam). Part (b) shows the corresponding horizontal windshear product.

Fig. 5. Damage of a (old) barn due to the tornado in Muiden on 23 August 2004 (photo by R. Sluijter).

thunderstorm has been observed by the Doppler weather radar in De Bilt at a range of about 30 km. Part (a) of Figure 6 shows the high-resolution radar reflectivity recorded at 1612 UTC and is zoomed in around Muiden. The supercell thunderstorm is clearly visible and a large band of extremely strong reflectivities (> 55 dBZ ≈ 100 mm/h) is seen. The hook echo, one of the most important signatures of a supercell, is located over Muiden.

Part (b) of Figure 6 shows the horizontal wind shear product corresponding to the high-resolution reflectivity product of part (a). Around the hook echo of the super cell, a region with strong horizontal wind shear (> 15 m s^{-1} km^{-1}) reflecting the mesocyclone of the supercell is evident. So the Doppler radar detected the mesocyclone associated with the tornado in Muiden. It is stressed that a Doppler weather radar cannot detect a tornado directly because it is too small and too close to the earth's surface.

VI. Monitoring of bird migration

Migrating birds are a potential hazard for aircrafts during take-off, landing, and low-level flights. The impact of a crash of a crane with a military helicopter flying at 300 meter altitude in Israel is shown in Figure 7. Furthermore migrating birds can cause severe errors in the wind speed (up to 20 m/s!) and direction retrieved from a Doppler radar.

Figure 1 shows two examples of VAD data from the radar in De Bilt. The upper frame displays a high-quality "wind" VAD during the passage of a cold front while the lower frame shows a VAD during intense bird migration. The huge difference in scatter of the observed radial velocity data around the modelled radial velocities is evident. The amount of scatter can be quantified using the standard deviation of the radial velocity (σ_r). Observations from a mobile bird radar of the Royal Netherlands Air Force (RNLAF) have been used to validate the discrimination of winds and birds using σ_r. These data have been recorded during the spring of 2003 at air force base De Peel, about 80 km from the radar in De Bilt.

A scatter plot of the reflectivity versus σ_r for the radar wind vectors of De Bilt is shown in Figure 8. The magenta and blue bullets correspond to vectors classified by the mobile bird radar

Fig. 7. A full hit of a crane on a military helicopter flying at 300 meter altitude in Israel. Cranes migrate in large numbers over Israel in March (photo obtained via RNLAF).

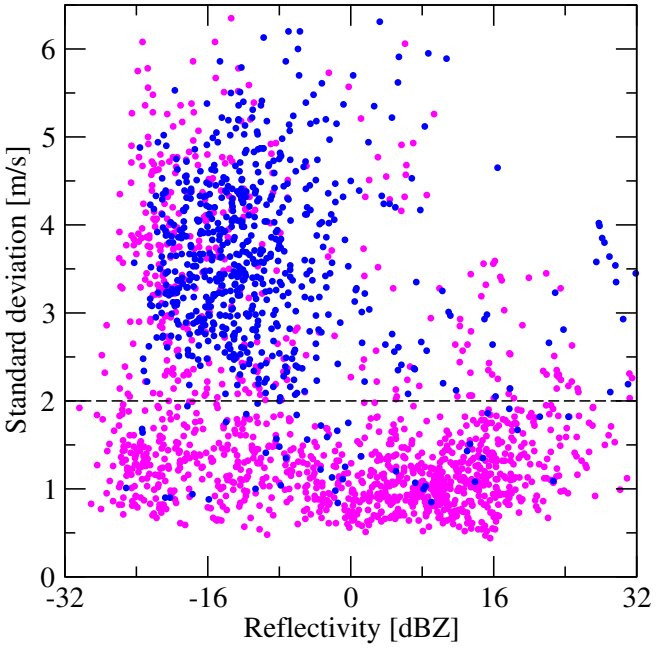

Fig. 8. A scatter plot of the reflectivity versus the standard deviation of the radial velocity (σ_r) for the radar wind vectors. The magenta bullets and blue bullets correspond to vectors classified by the mobile bird radar as "wind" and "birds", respectively.

in De Peel as "wind" and "birds", respectively. The horizontal dashed line marks the default threshold used to quality control the wind vectors. The excellent separation between wind and birds is evident from the figure. The magenta bullets above the dashed line are mostly due to insects. It is straightforward to use this method for the rejection of bird contamination from wind profiles (Holleman 2008), and further development will improve the extraction of bird migration information (Gasteren 2008).

VII. Outlook

Due to the EUMETNET programme on operational exchange of weather radar data (OPERA) the availability of weather radar wind profiles in Europe has increased dramatically, and the format and quality of the exchanged data have been harmonized. Operational assimilation of the wind data from the European radar network in the HIRLAM model will be pursued. In 2007 the receivers, signal processors, and control systems of the KNMI weather radars have been modernized. This upgrade enables higher update frequencies, higher spatial resolution, and new (Doppler) products.

Acknowledgements

Hans Beekhuis (KNMI) is gratefully acknowledged for his skilful technical assistance and good collaboration. The work on temperature advection from radar wind profiles has been performed by Susanne Jonker (WUR). Han Mellink (KNMI) helped with analysing the cases for the evaluation of the horizontal wind shear product. The collaboration with Hans van Gasteren (RNLAF) and prof. Willem Bouten (UvA) on the bird migration research is highly appreciated.

References

[1] Browning, K. A. and R. Wexler, 1968. The determination of kinematic properties of a wind field using Doppler radar. J. Appl. Meteor., 7,105-113.

[2] Gasteren, H. van, I. Holleman, W. Bouten, and E. van Loon, 2008. Extracting bird migration information from C-band weather radars. Ibis, in press.

[3] Holleman, I. and H. Beekhuis, 2003. Analysis and correction of dual-PRF velocity data. J. Atm. Oceanic. Technol., 20, 443-453.

[4] Holleman, I., 2005. Quality control and verification of weather radar wind profiles. J. Atm. Oceanic. Technol., 22, 1541-1550.

[5] Holleman, I., H. Mellink, T. de Boer and H. Beekhuis, 2005. Evaluatie van Doppler windscheringproduct (in Dutch). KNMI Internal Report IR 2005-01.

[6] Holleman, I., H. van Gasteren and W. Bouten, 2008. Quality Assessment of Weather Radar Wind Profiles during Bird Migration. J. Atm. Oceanic. Technol., submitted.

[7] Jonker, S., 2003. Temperature advection derived from Doppler radar wind profiles. KNMI Internal Report IR 2003-08.

[8] Waldteufel, P. and H. Corbin, 1979. On the analysis of single Doppler radar data. J. Appl. Meteor., 18, 532-542.